



# Along-strike variability of primitive magmas (major and volatile elements) inferred from olivine-hosted melt inclusions, southernmost Andean Southern Volcanic Zone, Chile

D.J. Weller\*, C.R. Stern

Dept Geological Sciences, University of Colorado, Boulder, CO 80309-0399, USA



## ARTICLE INFO

### Article history:

Received 14 July 2017

Accepted 9 November 2017

Available online xxxx

### Keywords:

Andean volcanism

Tephra

Olivine melt inclusions

Primitive magma

Volatiles

## ABSTRACT

Glass compositions of melt inclusions in olivine phenocrysts found in tephra derived from explosive eruptions of the four volcanoes along the volcanic front of the southernmost Andean Southern Volcanic Zone (SSVZ) are used to constrain primitive magma compositions and melt generation parameters. Primitive magmas from Hudson, Macá, and Melimoyu have similar compositions and are formed by low degrees (8–18%) of partial melting. Compared to these other three centers, primitive magmas from Mentolat have higher  $\text{Al}_2\text{O}_3$  and lower MgO,  $\text{TiO}_2$  and other incompatible minor elements, and are generated by somewhat higher degrees (12–20%) of partial melting. The differences in the estimated primitive parental magma compositions between Mentolat and the other three volcanic centers are consistent with difference in the more evolved magmas erupted from these centers, Mentolat magmas having higher  $\text{Al}_2\text{O}_3$  and lower MgO,  $\text{TiO}_2$  and other incompatible minor element contents, suggesting that these differences are controlled by melting processes in the mantle source region above the subducted oceanic plate. Parental magma S = 1430–594 and Cl = 777–125 ( $\mu\text{g/g}$ ) contents of Hudson, Macá, and Melimoyu are similar to other volcanoes further north in the SVZ. However, Mentolat primitive magmas have notably higher concentrations of S = 2656–1227 and Cl = 1078–704 ( $\mu\text{g/g}$ ). The observed along-arc changes in parental magma chemistry may be due to the close proximity below Mentolat of the subducted Guamblin Fracture Zone that could efficiently transport hydrous mineral phases, seawater, and sediment into the mantle, driving enhanced volatile fluxed melting beneath this center compared to the others.

© 2017 Elsevier B.V. All rights reserved.

## 1. Introduction

Along-arc variations in the composition of convergent plate boundary magmas may be related to various subduction parameters such as the age, thickness, thermal state, and composition of the subducting oceanic lithosphere, the volume and composition of the sediments entering the trench, and the age and composition of the mantle wedge. Understanding the mechanisms causing variations in the compositions of arc magmas requires constraining details of the processes of melt generation such as primitive magma compositions, volatile contents and melting parameters, details that are often lost during modification of primitive magmas during ascent, differentiation, and eruption. However, melt inclusions hosted in early formed phenocryst minerals such as olivine (Fig. 1) are a potentially valuable source of information on the composition of primitive magmas and the conditions of melt generation. Melt inclusions are small pockets of silicate melts trapped inside of phenocrysts at magmatic temperatures and pressures (Lowenstern, 1995; Wallace, 2005). The phenocrysts isolate the melt inclusions

from the ascending and evolving host magma limiting chemical exchange and to a degree, thermal interaction. Additionally, the phenocrysts prevent or at least retard degassing of the melt inclusions (Lowenstern, 1995). This has made melt inclusions a valuable source of information concerning the concentrations in magmas of magmatic volatiles such as  $\text{H}_2\text{O}$ , S, and Cl (Kelley et al., 2010; Portnyagin et al., 2007; Wallace, 2005; Wehrmann et al., 2014).

To better understand the along-strike geochemical variability observed in the eruptive products of the volcanoes Melimoyu, Mentolat, Macá, and Hudson, located along the volcanic front of the southernmost Andean Southern Volcanic Zone (SSVZ; Fig. 2), melt inclusions observed in olivines (Figs. 1 and 3) occurring in tephra deposits taken from lacustrine sediment cores that were derived from explosive eruptions of these volcanoes have been examined. For these arc-front volcanoes of the southernmost SSVZ, we present melt inclusion compositions, including volatile contents (S and Cl), which are fractionation-corrected back to the compositions of primitive magmas in equilibrium with mantle peridotite (olivine Fo90) in order to better understand the influence of subducting Nazca Plate features such as fracture zones on the primitive magma major and volatile element geochemistry during the early phase of magma evolution. Watt et al. (2013) previously

\* Corresponding author.

E-mail address: [derek.weller@colorado.edu](mailto:derek.weller@colorado.edu) (D.J. Weller).

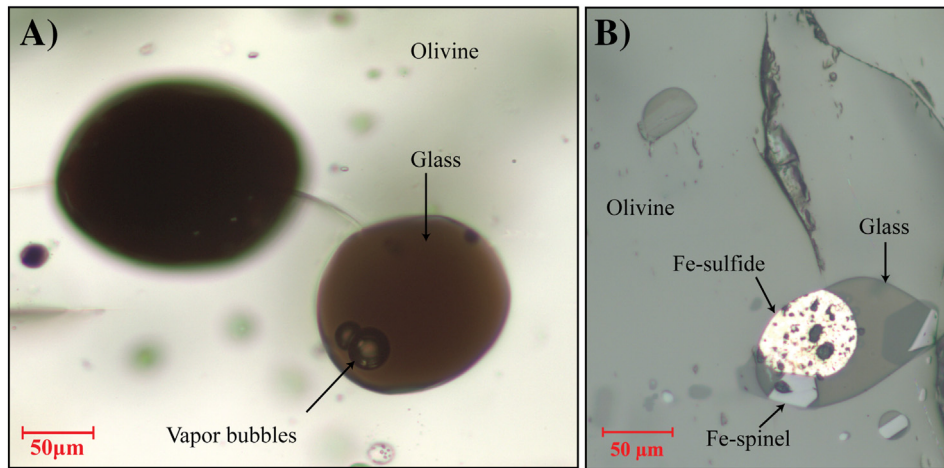


**Fig. 1.** A. Plane light photomicrograph of a typical Mentolat-derived melt inclusion (MEN4) analyzed in this study. Melt inclusions are generally homogenous with small vapor bubbles. B. Reflected light photomicrograph of a Macá-derived melt inclusion (MAC8) containing a Fe-sulfide and a Fe-rich spinel. Melt inclusion containing crystals were avoided, but provide information on the primary phases during early magmatic evolution. The large size of the minerals within their associated inclusion indicates that they were unlikely to form within the melt inclusion.

analyzed melt inclusions and calculated primitive parental magma compositions for volcanic centers further north in the Andean SSVZ and found a systematic across-arc change in the major, trace, and volatile element geochemistry in primitive magmas which were interpreted as temperature-dependent changes in the type of material (aqueous fluids or sediment melts) entering into the source region with progressive dehydration of the subducting slab. [Kratzmann et al. \(2010\)](#) also

presented compositional data for melt inclusions in plagioclase and pyroxene phenocrysts occurring within tephra derived from three large explosive Holocene eruptions of Hudson volcano, the southernmost center in the SSVZ, but the compositions of these inclusions were more evolved than the compositions of the bulk magmas and they were not interpreted to reflect or provide information about primitive parental magmas.

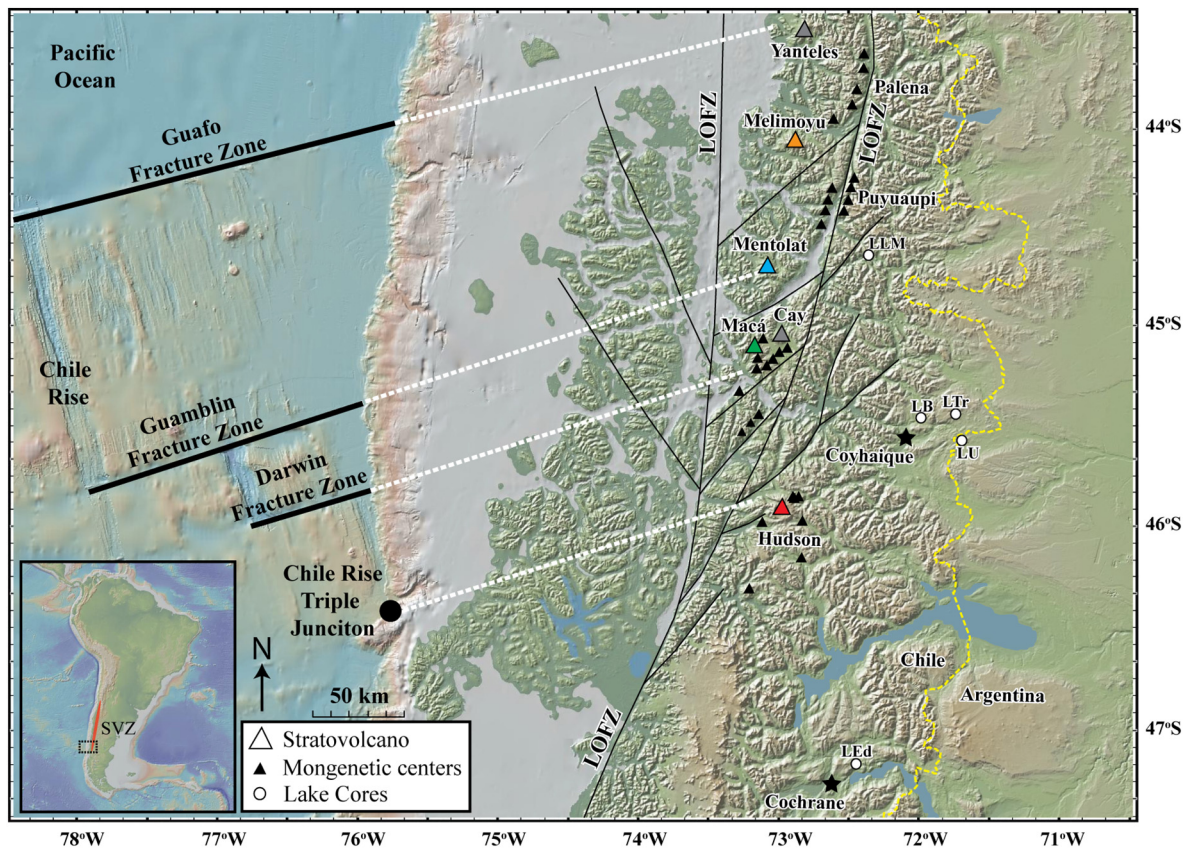


**Fig. 2.** Map of the southernmost portion of the Andean Southern Volcanic Zone showing the location of Hudson, Macá, Cay, Mentolat, Melimoyu, and Yanteles volcanoes. The volcanoes examined in this study are color coded with the same colors used in the subsequent figures. Also shown are the location of the small monogenetic eruptive centers (MEC) located along the Liqueñe-Oñqui Fault Zone (LOFZ; [Vargas et al., 2013](#)) and surrounding Hudson ([Gutiérrez et al., 2005](#)), Macá and Cay ([D’Orazio et al., 2003](#)), the location of the Chile Rise Triple Junction where the Chile Rise enters the trench, the location of some of the lake cores from which olivines were collected, and the location of Nazca Plate fracture zones with their projected location under the South American continent. Map was constructed using GeoMapApp (<http://www.geomapp.org>).

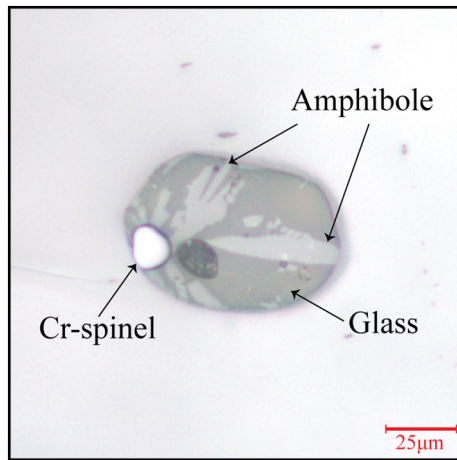


**Fig. 3.** Reflected light photomicrographs of an amphibole-bearing olivine-hosted melt inclusion derived from the H1 eruption of Hudson (Naranjo and Stern, 1998; Stern et al., 2016).

## 2. Geologic background

Volcanism in southern Chile occurs in two distinct zones, the Southern Volcanic Zone (SVZ; Fig. 2) and Austral Volcanic Zone (AVZ; Stern, 2004), resulting from the subduction of the Nazca (7 cm/yr) and Antarctic (1–2 cm/yr) plates beneath the South American continent (DeMets et al., 2010). The SVZ is an ~1400 km long volcanic chain consisting of 60 Quaternary stratovolcanoes, at least 3 large caldera complexes and numerous monogenetic eruptive centers (MEC; Stern, 2004). The SVZ is divided into four volcanic segments termed, from north-to-south, the northern (NSVZ), transitional (TSVZ), central (CSVZ), and southern (SSVZ) SVZ. The divisions of these segments are based on the geometry of the volcanic arc and the chemical characteristics of the erupted rocks, although the exact locations of the segment boundaries are still debated (Sellés et al., 2004; Völker et al., 2011).

This study focuses on melt inclusions in olivines collected from tephra derived from Melimoyu, Mentolat, Macá, and Hudson (Fig. 2). Hudson, which had a large explosive eruption in 1991 (Kratzmann et al., 2009), is the southernmost volcano of the SVZ and sits approximately 280 km east of the projected direction of the subducting Chile Rise. The point where the Chile Rise, an active spreading center separating the Nazca and Antarctic Plates, enters the trench is the Chile Rise-Trench Triple Junction (Fig. 2). Collision of the Chile Rise with the southernmost sector of South American occurred in the Miocene and due to the slight oblique subduction of the Nazca Plate, has migrated northward along the continental margin over the last ~14 Ma (Cande and Leslie, 1986). South of Hudson there is a >350 km gap in recently active volcanism separating the SSVZ from the AVZ (Stern, 2004).

The dominant tectonic feature in the region, the Liquiñe-Ofqui Fault Zone (LOFZ; Fig. 2; Cembrano et al., 1996), results from the oblique subduction of the Nazca Plate and the impingement of the Chile Rise against the continental margin (Cande and Leslie, 1986). Numerous small mafic monogenetic eruptive centers (MEC) occur along segments of the LOFZ (Fig. 2), but the large stratovolcanoes are located on blocks bounded by these segments. Hudson occurs to the east of the main LOFZ, while the other three centers occur west of the main fault. Another possibly significant tectonic feature is the Guamblin Fracture Zone on the Nazca Plate, the eastward projection of which occurs below Mentolat volcano (Fig. 2).

The volcanoes of the SSVZ ascend through relatively thin continental crust (~25–30 km; Völker et al., 2011) and despite isotopic evidence for only limited interaction with continental crust (D’Orazio et al., 2003; Futa and Stern, 1988; López-Escobar et al., 1993; Notsu et al., 1987), there is significant geochemical diversity amongst the volcanoes of the

southernmost SSVZ. López-Escobar et al. (1993, 1995) recognized these chemical differences and proposed a two-fold geochemical classification based on the relative abundances in basalts of  $K_2O$ ,  $Al_2O_3$  and incompatible trace element such as high-field-strength (HFSE; Ti, Zr, Nb, Hf, U), large-ion-lithophile (LILE; Cs, Rb, Ba, Sr, K, Th), and rare-earth-elements (REE). Amongst the volcanoes of the SSVZ, Hudson and Melimoyu produce mafic and intermediate lavas and tephra that have relatively high concentrations of  $K_2O$ , HFSE, LILE, and REE (Carel et al., 2011; Futa and Stern, 1988; Gutiérrez et al., 2005; Kratzmann et al., 2009, 2010), which corresponds to the Type-2 classification of López-Escobar et al. (1993, 1995) and have been termed High Abundance (HA) geochemical centers (Stern et al., 2015, 2016; Weller et al., 2014, 2015, 2017a). These are both relatively large volcanoes, with minimum volumes estimated at 147 and 142  $km^3$  respectively, compared to 100  $km^3$  for the average SVZ volcano (Völker et al., 2011). In contrast, Macá and Mentolat, which are both relatively small volcanic centers with volumes of 39 and 36  $km^3$  respectively, produce mafic and intermediate lavas and tephra with relatively low concentrations of  $K_2O$ , HFSE, LILE and REE (D’Orazio et al., 2003), which corresponds to the Type-1 classification of López-Escobar et al. (1993, 1995) and have been termed Low Abundance (LA) geochemical centers. However, Mentolat erupts lavas and tephra with exceptionally low concentrations of  $K_2O$ , HFSE, LILE and REE. It has therefore been further subdivided from the LA-type centers and is termed a Very Low Abundance (VLA) geochemical center (Stern et al., 2015, 2016; Weller et al., 2015, 2017a,b). It also differs from the other three centers by the presence of amphibole in its eruptive products. There are a few other centers further north in the SVZ that have erupted amphibole-bearing magmas with VLA geochemical characteristics including Huequi (Watt et al., 2011), Calbuco (Hickey-Vargas et al., 1995) and Nevado de Longaví (Rodríguez et al., 2007; Sellés et al., 2004).

These geochemical characteristics combined with tephra morphology and textural information (glass color, vesicle abundances and morphology, phenocryst type and abundance) have been used, along with tephra isopach maps, to identify source volcanoes for tephra derived from explosive eruptions from the SSVZ centers observed in outcrops (Naranjo and Stern, 1998, 2004; Stern, 2008), lakes and bogs (Elbert et al., 2013; Stern et al., 2015, 2016; Weller et al., 2014, 2015, 2017a,b) and Pacific Ocean sediment cores (Carel et al., 2011). Based on these characteristics, tephra produced by numerous explosive eruptions from each of these four SSVZ centers have been identified. These include: 1) for Hudson, a very large late-glacial (Ho; Weller et al., 2014) and two other large Holocene eruptions (H1, H2; Naranjo and Stern, 1998), as well as >25 other smaller eruptions (Weller et al., 2015, 2017a) prior to its most recent large explosive eruption in 1991 (H1991; Naranjo et al., 1993; Kratzmann et al., 2009); 2) for Macá, a late Holocene tephra in outcrop attributed to a medium sized explosive eruption (MAC1; Naranjo and Stern, 2004) that is also observed, along with 13 additional tephra that also may be attributed to eruptions of Macá, Cay, or one of the many MEC due to the similar geochemical characteristics, in lake cores near Coyhaique (Weller et al., 2015, 2017a); 3) for Mentolat, a large mid Holocene eruption (MEN1; Naranjo and Stern, 2004; Stern et al., 2016), as well as 12 other late-glacial and Holocene eruptions of Mentolat preserved as tephra in lake cores near Coyhaique (Weller et al., 2015, 2017a) and further north in the Río Cisnes valley (Stern et al., 2015; Weller et al., 2017a); and 4) for Melimoyu, two eruptions (MEL1 and MEL2; Naranjo and Stern, 2004) identified by tephra in outcrop, and three other late-glacial and Holocene tephra documented in lake cores in the Río Cisnes valley (Stern et al., 2015).

## 3. Samples

Olivines were selected from tephra preserved in sedimentary cores from lakes east of the SSVZ volcanoes (Fig. 2; Table 1) which have been the focus of tephrochronologic studies because of their exceptional

preservation of tephra derived from large and small explosive eruptions of the volcanoes of the SSVZ (Stern et al., 2015, 2016; Weller et al., 2015, 2017a,b). The cores were taken using a modified Livingstone piston corer at one meter intervals until the sediment transitioned from predominately organic matter-rich lacustrine sediments to glaciolacustrine clays and sands. Details of the lake cores, including the X-ray photographs, tephra geochemistry, and source volcano identification are reported by Weller et al. (2014, 2015, 2017a) and Stern et al. (2015, 2016). The transmitted X-ray photograph and the bulk tephra geochemistry for a previously undescribed core from Baguales lake (LB; Fig. 2) are presented in Fig. S1 and Table S1. The tephra in the LB core have been correlated based both on the stratigraphic relations and bulk tephra geochemistry with tephra in the other cores taken from the region.

All of the tephra deposits from which olivines were selected are derived from Holocene to late Pleistocene explosive eruptions of the four volcanoes along the volcanic front of the southernmost SSVZ. Each of these eruptive units contain unzoned olivine phenocrysts dislodged from the glass and are mixed in with other mineral phenocrysts and pumice fragments that range in compositions from mafic to more felsic. All of the observed tephra from Melimoyu, Mentolat, and Hudson have to some degree a bimodal character except the MAC1 eruption of Macá which only contains dark mafic material and lacks a felsic component. All of the tephra containing both mafic and felsic components, are mixed and lacking evidence for any sequential change in magma chemistry throughout the duration of the eruptive event. The deposition of these tephra within lacustrine systems acts to mix and eliminate any stratigraphic preservation of sequentially variable eruptive phases produced.

### 3.1. Hudson olivines

Olivine phenocrysts were selected from tephra produced by three of the four Holocene to late Pleistocene explosive eruptions of Hudson: H2, H1, and Ho (Table 1). These three eruptions of Hudson, as well as H1991, are similar in their mineral phenocryst phases. These tephra all contain phenocrysts of plagioclase, clinopyroxene, orthopyroxene and olivine, along with variable amounts of dense black mafic glass (Weller et al., 2014) and more felsic pumice lapilli. The olivines in the Hudson-derived tephra were collected from three different lake cores (Fig. 2; Table 1). The H2 tephra ( $\sim 3868 \pm 84$  cal years BP; Weller et al., 2017a) was taken from the lake Baguales core (LB; Fig. 2), the H1 tephra ( $\sim 7750$  cal years BP; Stern et al., 2016) from lake Edita (LEd) near Cochrane, and the Ho tephra ( $18,459 \pm 205$  cal years BP; Weller et al., 2014, 2015, 2017b) from lake Mellizas (LM) near Coyhaique.

### 3.2. Mentolat olivines

Throughout the Holocene, Mentolat has produced tephra consisting of abundant phenocryst of plagioclase, clinopyroxene, orthopyroxene, and amphibole (Weller et al., 2015). Only some of the Mentolat-derived tephra have abundant olivine phenocrysts. Great variability in the glass color and composition is observed in Mentolat tephra. Many

of the eruptive units contain fine white pumice lapilli ranging from dacite to rhyolite in composition (Weller et al., 2017a) and smaller proportions of dark grey mafic glasses. Olivine phenocrysts were selected from three Holocene eruptions each taken from different lake cores (Table 1). These eruptions include the tephra B2 ( $1426 \pm 367$  cal years BP; Weller et al., 2017a) from lake Tranquillo (LTr; Fig. 2), tephra D1 ( $1774 \pm 216$  cal years BP) from lake Unco (LU), and tephra I ( $>5151$  cal years BP) in lake Las Mellizas (LLM) from the Río Cisnes valley east of Mentolat (Weller et al., 2017a).

### 3.3. Macá olivines

Macá has only produced one regionally widespread tephra deposit (MAC1;  $\sim 1922 \pm 215$  cal years BP; Naranjo and Stern, 2004; Weller et al., 2015, 2017b). This tephra is predominately black to dark brown in color with a basaltic-andesite bulk rock composition (Naranjo and Stern, 2004) and olivine, clinopyroxene, and plagioclase are the dominant phenocrysts. The olivines were selected from this tephra in the lake Baguales core (LB; Fig. 2; Table 1).

### 3.4. Melimoyu olivines

Melimoyu tephra generally consist of phenocryst of plagioclase, orthopyroxene, clinopyroxene, and olivine. The Melimoyu derived olivine phenocrysts were picked from the MEL2 tephra ( $\sim 1680$  cal years BP) of the lake Las Mellizas (LLM; Table 1) core taken from the lower reaches of the Río Cisnes valley (Fig. 2; Weller et al., 2017a). MEL2 tephra has black to light brown glass and pumice with an andesitic bulk rock composition (Naranjo and Stern, 2004).

## 4. Methods

Olivines occur as phenocrysts dislodged from the glass and were hand-picked from the tephra deposits, mounted in epoxy and polished to expose melt inclusions. Melt inclusion and mineral phenocryst major element contents were determined using a Jeol JXA-733 Electron Microprobe that was operating at 15 KV accelerating potential with a 5 nA probe current for the glasses and 20 nA probe current for the mineral phenocryst. Ten second counting time were used for the elements Na, Mg, Si, Al, Ca, K, Ti, Cl, and S. Fe and Mn were analyzed at 15 s counting times, Cr at 20 s, and P at 25 s. Basaltic glass standard USNM #113498/1 was used for the analyses of the melt inclusions. Volatile elements were analyzed early in the analysis sequence and a defocused beam was used to minimize loss of volatile elements such as Na and Cl from the melt inclusion glasses. The analyses of the melt inclusions from each volcano were performed contemporaneously over a three-day period with good analytical reproducibility between each session and within the individual melt inclusions. Repeat analyses were performed on each inclusion and their host olivine phenocrysts. Some olivine phenocrysts contained multiple inclusions that were treated as independent and not averaged with other inclusions from the same olivine. Water contents of the melt inclusions were estimated by the difference method assuming all of the missing component in the analyses was H<sub>2</sub>O. We stress that determining the H<sub>2</sub>O contents of silicate glasses by the difference method is

**Table 1**  
Information for the olivine-bearing tephra deposits used in this study.

Eruption	Source	Lake	Latitude S	Longitude W	Core	Section	Depth (cm)	Age (cal yrs BP)	Error
MEL2	Melimoyu	Laguna Las Mellizas	44°39'01.1"	72°19'50.41"	0115B	BT2	46–49	~1680	–
B2	Mentolat	Tranquillo	45°27'29.1"	71°44'43.1"	PC1203	AT3	0–4	1,426	367
D1	Mentolat	Unco	45°34'29.4"	71°43'7.6"	PC1103	ET1	94–95	1,774	216
I	Mentolat	Laguna Las Mellizas	44°39'01.1"	72°19'50.41"	0115B	BT3	86–92	>5,151	–
MAC1	Macá	Baguales	45°29'53.7"	71°55'5.6"	PC1104	AT1	21–30	1,922	215
H2	Hudson	Baguales	45°29'53.7"	71°55'5.6"	PC1104	AT1	66–74	3868 ± 84	–
H1	Hudson	Edita	47°9'5.40"	72°21'12.50"	PC0902	AT7	20–38	7689 ± 23	–
Ho	Hudson	Las Mellizas	45°32'31.9"	71°48'32.3"	PC1106	AT6	0–55	18,459	205

imprecise, and has uncertainties because electron microprobe deficits may be related to a number of other factors in addition to the H<sub>2</sub>O content, most notably, the loss of other volatile species such as CO<sub>2</sub>, F, and the migration of Na (Morgan and London, 1996) throughout the analysis sequence. Even when the microprobe conditions are optimized to reduce the loss of volatiles, the difference method can still yield 1 wt% difference in the water contents in comparison to directly measured techniques (Devine et al., 1995; King et al., 2002).

#### 4.1. Melt inclusion post-entrapment modifications

After entrapment of a melt inclusion, crystallization of olivine along the wall of the inclusion can occur, which will remove olivine constituents from the glass. We corrected for this post-entrapment crystallization (PEC) by adding increasingly forsteritic olivine back into the melt inclusion at 0.01% increments until the melt inclusion is in equilibrium with the forsterite content of the core of the host olivine (Table S2). These corrections are carried out using the Petrolog software (Danyushevsky and Plechov, 2011) with the olivine melt equilibrium model of Ford et al. (1983).

Additionally, after entrapment, the melt inclusion can be further modified by diffusive re-equilibration with the host olivine. Danyushevsky et al. (2000, 2002) observed that melt inclusion compositions were modified by diffusive exchange of Fe out of the melt inclusion. The loss of Fe can be recognized by lower FeO\* (FeO as total Fe) values in the melt inclusion compared to the whole rock FeO\* versus MgO trend of the host magma. The degree of Fe lost by diffusion in the melt inclusion is usually greatest in the most MgO-rich olivines (Danyushevsky et al., 2002). To assess for Fe-loss, we used two methods. First, we compared uncorrected melt inclusion FeO\* vs. host olivine Fo content. Additionally, we compared the FeO\* fractionation trend for the melt inclusion with published whole rock and bulk tephra analyses for SSVZ volcanoes following the method of Danyushevsky et al. (2000). These comparisons suggest that some of the melt inclusions have experienced varying degrees of Fe-loss, particularly for those within olivines from Hudson and Melimoyu, but less so for the Mentolat and Macá inclusions.

Previous melt inclusion studies recognized and corrected for Fe-loss by diffusive exchange with the host olivine by comparing the FeO content of the melt inclusion and bulk rock (Danyushevsky et al., 2002). However, due to the heterogeneous nature of these tephra, which represent the end processes of mixing and setting within the lakes themselves, and also segregation of material during areal transport, it is difficult to know what the bulk whole rock composition of these tephra was originally. Additionally, previously published bulk tephra analyses for many of these tephra including the H1 and H2 events of Hudson (Naranjo and Stern, 1998), the MEL2 eruption of Melimoyu, and the MAC1 eruption of Macá (Naranjo and Stern, 2004) are more evolved than the melt inclusion glass compositions. Thus, bulk tephra analyses are not useful to assess for the degree of Fe-loss. Instead, to correct for diffusion related re-equilibration, the FeO\* content of the melt inclusions are corrected to the average of the highest melt inclusion FeO\* in other olivines from the same volcanoes deemed to be unaffected or least affected by diffusion related Fe-loss (Table S3). At Melimoyu, there wasn't sufficient data available for this determination and a different method was used to correct for diffusion related Fe-loss. First, the melt inclusions were corrected for PEC without modifying the original FeO\* contents. After this correction, a comparison of MgO vs FeO\* indicated that the melt inclusion FeO\* contents were significantly lower than the liquid lines of descent defined by previously published lava samples from Melimoyu (López-Escobar et al., 1993) indicating that some degree of Fe-loss had occurred. Therefore, the melt inclusion FeO\* contents were corrected to the whole rock fractionation trend at the MgO contents of the PEC-corrected melt inclusions.

Melt inclusion can also lose volatile gasses by diffusion, formation of vapor bubbles, and by rupturing of the host crystal (Wallace, 2005). Two

criteria were used to assess for melt inclusion degassing. If the PEC and Fe loss-corrected melt inclusion failed either of these criteria, they were excluded from further modeling (Table S3). Melt inclusions with PEC and Fe-loss corrected S content below 500 µg/g were deemed to be degassed following the criteria established by Kelley et al. (2010) and therefore are excluded from further modeling. Additionally, PEC and Fe loss-corrected melt inclusions with water contents < 1.5 wt% after PEC-correction were discarded because they have likely lost water and other volatiles and produced unrealistic results after performing the PEC-correction and reverse crystallization calculations. Table 2 summarizes the host olivine and melt inclusion information including the number of inclusions and data points analyzed from each eruption prior to, and after data filtering.

#### 4.2. Parental magma composition

The least degassed PEC and Fe loss-corrected melt compositions were fractionation-corrected back to primary melts in equilibrium with mantle olivine (Fo90; Stolper and Newman, 1994) by incrementally adding equilibrium olivine and/or clinopyroxene to each inclusion composition until mantle equilibrium is reached (Table S4). These calculations are performed using Petrolog in increments of 0.01% carried out at 1 kbar and a QFM + 1 buffer using the olivine-melt equilibrium model of Ford et al. (1983) and a clinopyroxene-melt equilibrium model of Ariskin et al. (1993). To assess for the *syn*-crystallization of other phases prior to melt entrapment, we examined major element trends in CaO, Al<sub>2</sub>O<sub>3</sub>, and MgO for the PEC-corrected melt inclusion (Fig. 4). The data suite for each volcanic center show variations consistent with the fractionation of olivine at all the centers, and clinopyroxene at Mentolat, Macá, Hudson, but not Melimoyu. None of the melt inclusions preserve evidence for significant plagioclase fractionation as seen by their nearly constant Al<sub>2</sub>O<sub>3</sub> contents with decreasing MgO (Fig. 4). High water contents are likely to suppress the crystallization of plagioclase at these MgO contents. Clinopyroxene saturation is indicated by the slight downward trend in CaO with decreasing MgO initiated at different MgO contents for each center and thus we apply the olivine-clinopyroxene cotectic up to these specified MgO contents after which olivine is assumed to be the only liquidus phase (Table S3).

The amount of olivine and clinopyroxene addition varied between the different centers but as a whole, the suite of data required an average olivine addition of ~20% which ranged to as high as 24% and as low as 12% (Tables S3 and S4). These values are similar to the average olivine addition made to estimate primitive magma compositions from the melt inclusion in olivine from the Marians arc (Kelley et al., 2010), lower than the average for volcanoes further north in the Andean SVZ (Wehrmann et al., 2014), and greater than was required for Hornopirén and the small monogenetic centers Apagado, South Minchinmávida, and Palena located just to the north in the Andean SSVZ (Watt et al., 2013). Where clinopyroxene addition is necessary, the average is generally low (~5%), with the exception of Hudson that required up to 19% addition of clinopyroxene.

To calculate the S and Cl contents of the primitive magmas, the original volatile contents (Table S2) were first corrected for post-entrapment crystallization and then back calculated to primitive compositions by treating the volatile elements as perfectly incompatible and utilizing the percent olivine and clinopyroxene required for the post-entrapment crystallization correction and the fractionation correction (Tables S2 and S4).

#### 4.3. Melting parameters

To better understand the influence of subducting Nazca Plate features such as fracture zones on the primitive magma and the processes contributing to the geochemical variability observed between the major centers of the SSVZ, we utilize models developed at other volcanic arcs

**Table 2**

Summary of host olivine, tephra deposits, and melt inclusion information used to calculate primitive magma compositions.

Eruption	Source	Olv. Fo range	Bulk tephra composition	No. inclusions	No. analyzed data pts.	No. olv. used in modeling	No. inclusion used in modeling	No. data pts. used in modeling <sup>a</sup>
MEL2	Melimoyu	82–84	Andesitic <sup>b</sup>	3	7	2	3	7
B2	Mentolat	79–82	–	4	13	3	4	13
D1	Mentolat	75–81	–	4	11	3	4	11
I	Mentolat	74–76	–	4	11	2	2	7
MAC1	Macá	74–84	Basaltic-Andesite <sup>b</sup>	10	32	8	10	32
H2	Hudson	79	Dacitic <sup>c</sup>	2	6	1	1	3
H1	Hudson	79–84	Andesitic <sup>c</sup>	5	14	3	5	14
Ho	Hudson	74–84	–	14	44	8	9	30

Olv.-olivine.

<sup>a</sup> Number of data points prior to averaging.<sup>b</sup> Naranjo and Stern (2004).<sup>c</sup> Naranjo and Stern (1998).

to estimate parameters such as fraction of mantle melting ( $F_m$ ) and source mantle water content. ( $C_{H_2O}^0$ ; Kelley et al., 2006), that can provide both a means of comparison of the conditions during melt generation below the different SSVZ centers and can also be used to compare to other volcanic arcs. The concentration of incompatible minor elements are useful for evaluating mantle melting processes. At a low percent of melting, the magma will have relatively high concentrations of incompatible elements. As the melt fraction increases, their concentrations in the melt progressively decrease as they are diluted by the addition of other material into the melt. Because of this simple behavior, the glass  $TiO_2$  can be used as a mantle melt fraction ( $F_m$ ) proxy (Kelley et al., 2006). Solving the batch melting equation in terms of  $TiO_2$ ,  $F_m$  can be estimated by making an assumption of the mantle Ti concentration (Kelley et al., 2006). Similarly, recasting the batch melting equation in terms of water and utilizing  $F_m$  from the previous formulation allows for the determination of the mantle source water content ( $C_{H_2O}^0$ ).

One of the major uncertainties in this formulation is therefore the original mantle  $TiO_2$  content. A normal mid-ocean ridge basalt (NMORB) mantle source has a value of 0.133 wt% (Salters and Stracke, 2004). This value may also be appropriate for the mantle below the Andean volcanic arc because Ti is likely to be retained in residual rutile and therefore unlikely to be added to the mantle wedge during dehydration of the subducting slab. However, using Ti and Y systematics, the source mantle  $TiO_2$  content has been estimated as being somewhat higher than MORB-source mantle for the region just north in the SSVZ (Watt et al., 2013), with a range of values between 0.162 and 0.196 wt%. To generate estimates for the mantle melt fraction ( $F_m$ ) and mantle water content ( $C_{H_2O}^0$ ), we have therefore used the two end member values of  $TiO_2 = 0.133$  wt% estimated for an NMORB

source mantle and 0.196 wt% estimated by Watt et al. (2013) for the mantle further north below the Andean SSVZ arc.

## 5. Results

Included in the results in Table S2 are the host-olivine compositions, the measured compositions for the individual olivine-hosted melt inclusions, and the PEC-corrected melt inclusion compositions (Figs. 5 and 6). In Table S4 are the primitive mantle melt compositions which are the fractionation corrected composition of the melt inclusion in equilibrium with mantle (Fo90) olivine (Fig. 6) and include the primitive melt  $H_2O$ , S and Cl contents. Table S5 includes the results for the mantle melting models using the NMORB source mantle Ti content and the estimated source mantle Ti content for the region north in the Andean SSVZ (Watt et al., 2013). In Table S6 are the compositions of the silicate mineral assemblages observed as crystals contained in the melt inclusions or in the olivines themselves.

### 5.1. General results

The melt inclusions are generally homogenous and contain either a single vapor bubble or no vapor bubbles (Fig. 1). The vapor bubbles likely formed as a result of decompression during ascent and eruption. Some of the inclusions contained crystals that were determined to be crystallizing pre- or syn-entrapment rather than post-entrapment due to their large size with respect to the associated melt inclusion (Figs. 1 and 3). Melt inclusion containing large microphenocrysts were avoided but they provide important information on early fractionating phases (Fig. 1). However, a few melt inclusions contained small partially

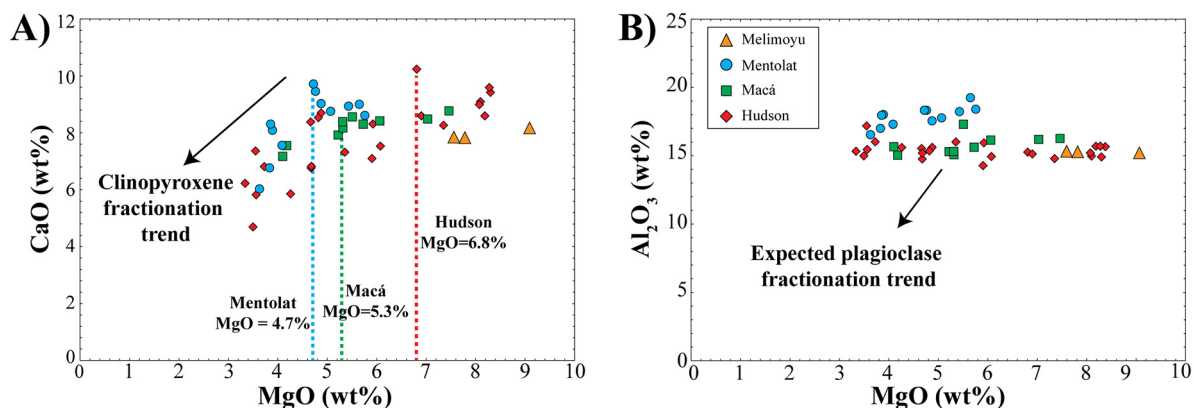


**Fig. 4.** Major element variation diagrams for A) CaO vs MgO and B)  $Al_2O_3$  vs MgO in weight percent oxide (wt%) for the post-entrapment crystallization-corrected (PEC) melt inclusions compositions. Clinopyroxene saturation occurs at different MgO contents for each center while significant plagioclase fractionation didn't occur prior to melt entrapment. Dashed lines indicate the point at which clinopyroxene saturation occurs, indicated by the slight decreasing CaO content at lower MgO values for Mentolat, Macá, and Hudson. Significant clinopyroxene fractionation is not observed at Melimoyu. The nearly constant  $Al_2O_3$  with decreasing MgO content indicates that plagioclase is not an important fractionating phase prior to the entrapment of the melt inclusions.

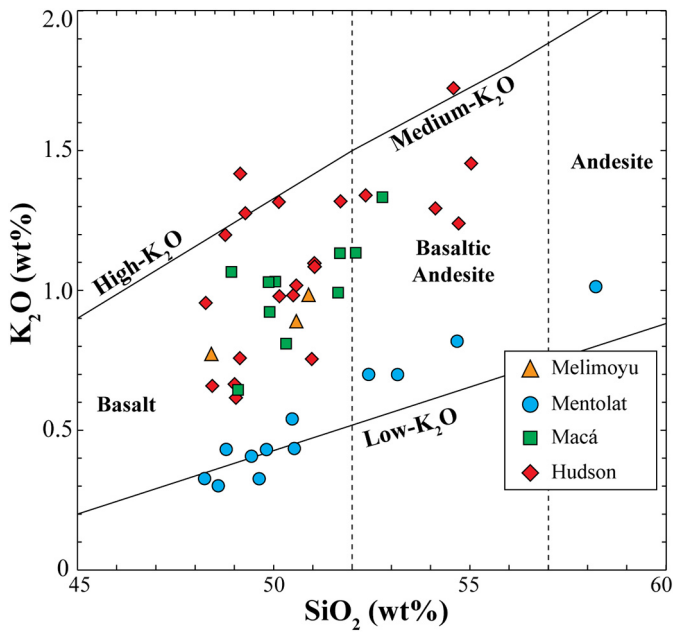


**Fig. 5.**  $K_2O$  versus  $SiO_2$  in weight percent oxide (wt%) diagram showing the range of compositions of the post-entrapment crystallization-corrected melt inclusion compositions for each volcanic center. Melimoyu, Macá, and Hudson generally have greater  $K_2O$  content at a given  $SiO_2$  than Mentolat, which is a Very Low Abundance (VLA)-type volcanic center. Geochemical classification lines are those of Ewart (1982).

crystallized phases which are not considered to significantly alter the melt inclusion composition after entrapment. All of the olivines analyzed in this study are considered to be primary and not xenocrysts.

After data filtering, the host olivine phenocrysts from the three Hudson eruptions (Ho, H1 and H2; Table 1) range in forsterite content from Fo74 to Fo84 (Tables 2 and S2) and occasionally contain microphenocrysts of Cr-spinel, ilmenite and in a few instances, Ca-rich plagioclase. One melt inclusion from the H1 eruption of Hudson contains elongated lath shaped amphiboles occurring together with a Cr-spinel crystal (Fig. 3). Amphibole has never been previously observed in any Hudson derived lavas (López-Escobar et al., 1993) or tephras (Kratzmann et al., 2009, 2010; Stern et al., 2015; Weller et al., 2014, 2015). The amphibole, which is hosted in an olivine with a forsterite content of Fo82, is a kaersutite (Table S6) according to the classification of Leake et al. (1997). Despite the absence of amphibole as a stable phase in the eruptive products of Hudson, decreasing Dy/Yb ratio with increasing differentiation in Hudson magmas has been interpreted as a chemical indicator for amphibole crystallization at depth (Davidson et al. 2007; Kratzmann et al., 2010; Weller et al., 2014). The olivine-hosted amphibole-bearing melt inclusion is therefore of significance because it is consistent with the suggestion that amphibole may be an important cryptic fractionating phase during the early magmatic evolution of Hudson magmas, although it has not been previously observed in any Hudson samples.

Melimoyu host olivine phenocrysts from one eruption (MEL2; Table 1) range only between Fo82 and Fo84 and also occasionally contain Cr-spinel and ilmenite (Tables 2 and S2). The host olivines from

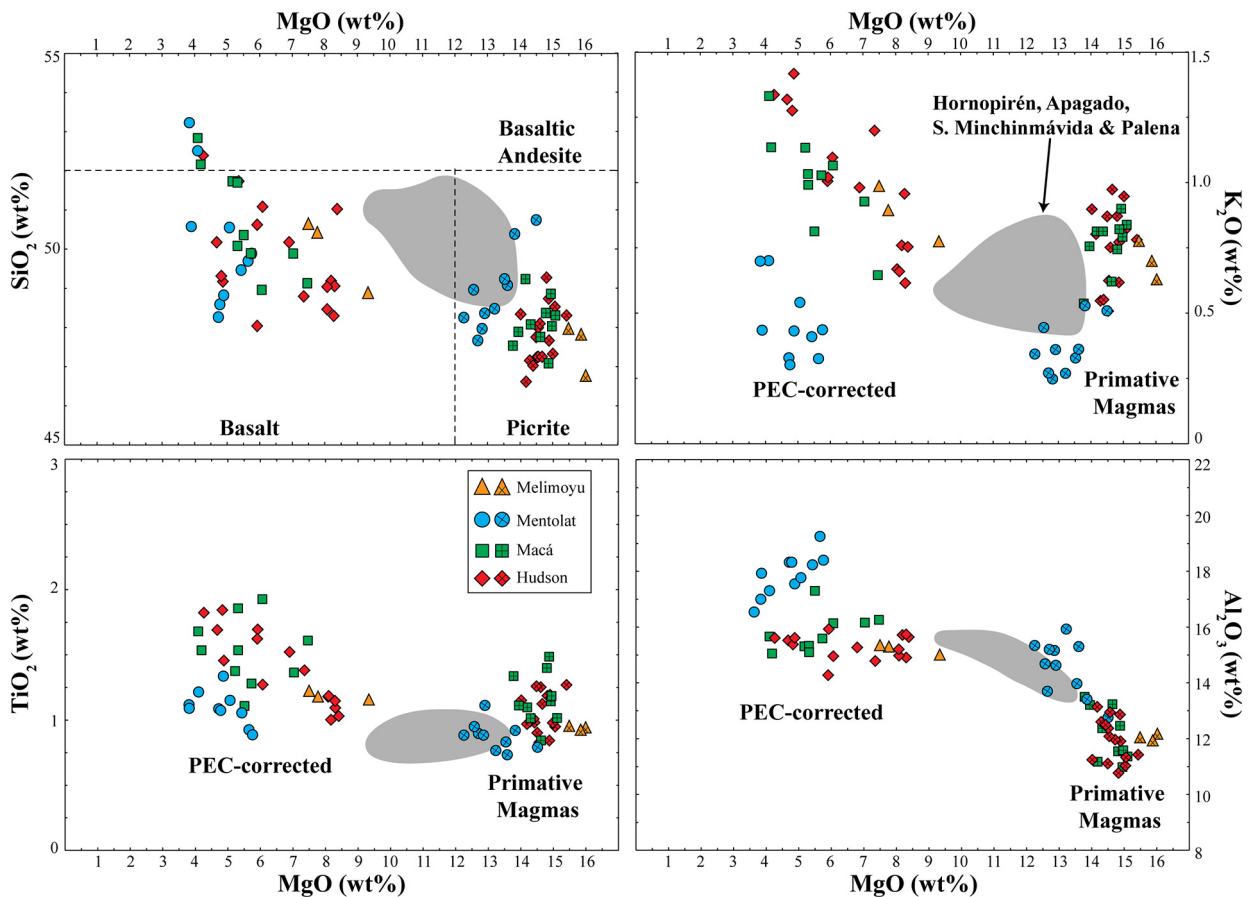


**Fig. 6.** Major element variation diagrams for the primitive magmas (symbols with cross or plus sign) and the PEC-corrected melt inclusion (open symbols) illustrating the geochemical variability observed in the primitive magmas, the PEC-corrected magmas from the southernmost SSVZ centers. Mentolat generally has lower  $K_2O$ ,  $TiO_2$ ,  $MgO$ , and higher  $Al_2O_3$  than the other centers that generally overlap in their magma compositions. Included for comparison are the compositional fields for primitive magma compositions determined for Hornopirén, and the mafic monogenetic centers north of the SSVZ centers (Watt et al., 2013).

three different Mentolat tephra (B2, D1 and I; Table 1) range in forsterite content from Fo74 to Fo82 (Table 2) and occasionally contain microphenocrysts of ilmenite, Ca-rich plagioclase (Table S6), Fe-spinel, and an unidentified Fe-sulfide. Similarly, the host olivine phenocrysts from the MAC1 eruption of Macá (Table 1) range in forsterite content between Fo74 and Fo84 (Table 2). A few of these olivines contain microphenocrysts of Fe-spinel, ilmenite, and an unidentified Fe-sulfide (Fig. 1). Matrix glass from one olivine phenocryst from Macá was analyzed for comparison with the melt inclusion composition (Table S6). The matrix glass is more evolved than the melt inclusion glasses (Table S6) consistent with the entrapment of less evolved magma compositions than the host magma.

The PEC-corrected melt inclusions for all the volcanoes range from 48 to 58 wt% SiO<sub>2</sub> while Macá and Melimoyu inclusions range only from 49 to 53 and 48–51 wt% SiO<sub>2</sub> respectively (Fig. 5; Table S2). Those from Hudson, Macá and Melimoyu are all medium- to high-K<sub>2</sub>O basalts and basaltic-andesites. Those from Mentolat are low- to medium-K<sub>2</sub>O calc-alkaline compositions that range from basalt up to andesitic in composition, consistent with the VLA character of magmas erupted from this volcano.

## 5.2. Parental magmas

Major element variation diagrams of the parental magma estimates from the least degassed melt inclusions (Table S3) from each center are shown in Fig. 6. For comparison, the PEC-corrected melt inclusion are also included, as well as fields for primitive magmas estimated from melt inclusions for Hornopirén, Apagado, Minchinmávida and the Palena volcanic centers further north in the SSVZ (Watt et al., 2013).

The primitive magmas of Hudson, Melimoyu, and Macá are generally all similar to each other and extend to higher parental magma MgO<sub>(90)</sub> (the MgO of primitive magma in equilibrium with mantle olivine with Fo90) compared to the primitive magma compositions determined for the volcanoes further north in the Andean SVZ (Fig. 6; Watt et al., 2013). However, Mentolat is distinct from the other centers in having lower MgO<sub>(90)</sub> contents for a given SiO<sub>2(90)</sub> content. Furthermore, other geochemical characteristics identified both in the more evolved tephra and the PEC-corrected melt inclusions of Mentolat are also present in the primitive magma compositions (Fig. 6), so that, for example, Mentolat primitive magmas have higher Al<sub>2</sub>O<sub>3(90)</sub> and lower K<sub>2</sub>O<sub>(90)</sub>, and TiO<sub>2(90)</sub> compared to the other SSVZ centers. The primitive magmas estimated from tephra B1 and D1 (Tables 1 and S4) are similar and overlap in the major elements compositions while the primitive magma estimates of tephra I of the Río Cisnes valley (Weller et al., 2017a) are slightly more evolved, and for a few elements, overlap with the primitive magma compositions from the other centers but still have the general VLA character of Mentolat derived tephra (Fig. 6).

## 5.3. Melting parameters

Compared to Mentolat, the fraction of melting ( $F_m$ ) is generally low for Hudson, Melimoyu and Macá, with an average of 9–16%, 11–18% and 8–14%, respectively, depending on the assumed mantle Ti content (Table S5, Fig. 7). Mentolat primitive magmas form from generally higher mantle melt fractions of 12–20%. The mantle water content  $C_{H_2O}^o$  is on average uniform for Hudson, Macá, and Melimoyu at ~0.22–0.40 wt% while the mantle beneath Mentolat is somewhat richer in water with an average  $C_{H_2O}^o$  of 0.33–0.52 wt%.

## 5.4. Volatiles

There is great variability in the volatile contents of the primitive magmas amongst the different volcanic centers and within the individual centers themselves (Fig. 8B). Mentolat has the greatest parental magma volatile content of all the centers, ranging from 2569 to 1215  $\mu\text{g/g}$  S<sub>(90)</sub> and 1078–704  $\mu\text{g/g}$  Cl<sub>(90)</sub>. Hudson also has large variations

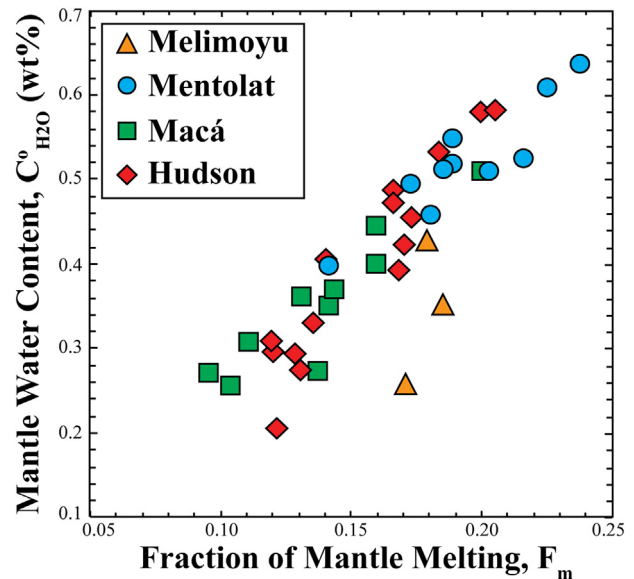


Fig. 7. Fraction of mantle melting ( $F_m$ ) versus Mantle water content ( $C_{H_2O}^o$ , wt% oxide) calculated using melting models of Kelley et al. (2006) and the  $C_{Ti}^o = 0.196$  wt% estimate of Watt et al. (2013) for the least degassed melt inclusions from the four southernmost volcanoes of the Andean SSVZ. The melting parameters for Melimoyu, Macá, and Hudson are generally similar and lower than the melting parameters for Mentolat. Compared to the other centers, primitive magmas from Mentolat form from generally higher degrees of partial melting of a more water rich mantle.

but with a much lower upper limit on the S<sub>(90)</sub> and Cl<sub>(90)</sub> content, ranging from 1320 to 594  $\mu\text{g/g}$  and 777–336  $\mu\text{g/g}$  respectively. Macá and Melimoyu overlap considerably, having a range of 1430–660 and 993–693 for S<sub>(90)</sub> and 701–125  $\mu\text{g/g}$  and 626–471  $\mu\text{g/g}$  for Cl<sub>(90)</sub> respectively.

## 6. Discussion

### 6.1. Parental magma compositions

Our estimates for the parental magma compositions are similar to other primitive magma compositions estimated from the region (Fig. 6; Watt et al., 2013) to the extent that they are all picrites. However, the four southernmost SSVZ centers along the volcanic front have some significant variability in their MgO<sub>(90)</sub> contents, mantle partial melting  $F_m$  and mantle source H<sub>2</sub>O contents in that Mentolat has lower MgO<sub>(90)</sub> contents than the other centers, and the highest  $F_m$  and  $C_{H_2O}^o$  (Fig. 7). This is consistent with the lower incompatible K<sub>2</sub>O and TiO<sub>2</sub> content of Mentolat magmas, which could result from the higher degrees of partial melting below Mentolat, thus diluting the concentration of these elements.

Another important point is that some of the distinctive geochemical characteristics present in the primitive parental magmas for Mentolat, such as relatively low MgO, K<sub>2</sub>O and high Al<sub>2</sub>O<sub>3</sub>, are also preserved in the more evolved lavas and tephra erupted from Mentolat. The other centers have a common primitive parental composition distinct from that of Mentolat (Fig. 6). This observation has two implications for these volcanoes: 1) primitive magmas from Mentolat are compositionally distinct at generation and thus sub-arc processes acting at the time of formation are likely responsible for this variability; and 2) the similarity in the parental melts from Hudson, Macá, and Melimoyu suggest that different diversification pathways after initial melt generation may be the cause for the geochemical diversity observed in their eruptive products, Macá erupting Type-1 low abundance (LA) magmas, while Hudson and Melimoyu erupt Type-2 high abundance (HA) magmas.

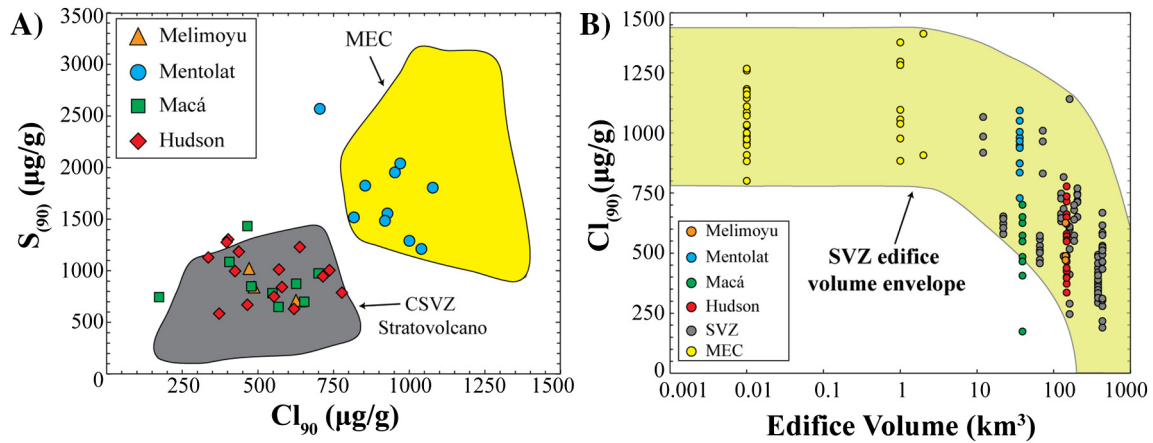


**Fig. 8.** A)  $S_{(90)}$  and  $Cl_{(90)}$  contents ( $\mu\text{g/g}$ ) for the southernmost SSVZ centers and fields for small ( $<10\text{ km}^3$ ) MEC (yellow field) and other larger stratovolcano ( $>20\text{ km}^3$ ) Central SVZ (CSVZ; grey field) centers of Wehrmann et al. (2014) for comparison. The primitive  $S_{(90)}$  and  $Cl_{(90)}$  contents of Melimoyu, Macá, and Hudson are similar to primitive magma  $S_{(90)}$  and  $Cl_{(90)}$  contents measured in olivine melt inclusion from the CSVZ stratovolcanoes, while the  $S_{(90)}$  and  $Cl_{(90)}$  contents from Mentolat are higher than the other SSVZ centers and are more similar to the MEC. B) Melt inclusions  $Cl_{(90)}$  content versus volcano edifice size ( $\text{km}^3$ ; Völker et al., 2011) for the least degassed melt inclusions from both MEC and SVZ stratovolcano centers. The small MEC (yellow symbols) have the greatest  $Cl_{(90)}$  contents while the  $Cl_{(90)}$  contents are strongly diluted at the larger centers, including Hudson and Melimoyu ( $\sim 100\text{ km}^3$ ) in the SSVZ. Mentolat ( $\sim 36\text{ km}^3$ ) has the highest  $Cl_{(90)}$  contents of all the SSVZ and CSVZ centers, but fits within the  $Cl_{(90)}$  versus edifice volume field of Wehrmann et al. (2014). (For interpretation of the references to color in this figure legend, the reader is referred to the web version of this article.)

## 6.2. Volatiles

### 6.2.1. Sulfur

Understanding the behavior of sulfur in magmatic systems has been a longstanding challenge due to the multiple valance states of sulfur and the sensitivity of sulfur speciation to changing oxygen fugacity ( $fO_2$ ), magma temperature, and melt composition (Wallace, 2005). In general, the S contents in arc magmas decrease with increasing differentiation that may be caused by the fractionation of S-bearing phases or potentially changes in pressure, temperature and magma composition which effects the solubility of S leading to devolatilization (Wallace and Edmonds, 2011).

Even in melt inclusions, the sulfur content can be modified by post entrapment effects caused by the diffusive re-equilibration of  $\text{FeO}^*$  with the host olivine. Danyushevsky et al. (2002) demonstrated that melt inclusions that experienced significant diffusion related Fe-loss can precipitate sulfides due to the decreased solubility of S. Indeed, melt inclusions from Mentolat and Macá both contain Fe-sulfides within the glass and embedded within the host olivine phenocryst (Fig. 1B). However, these centers were determined to be the least impacted by diffusive re-equilibration and thus these Fe-sulfides may also possibly represent primary phases during early magmatic evolution and not the result of re-equilibration processes. Furthermore, the relatively large size of the phases with respect to the associated inclusion, and the euhedral form of the spinel, supports their formation out of a larger volume of magma prior to entrapment within the melt inclusion (Fig. 1B).

In the Andean SVZ, Wehrmann et al. (2014) observed the highest S contents, measured from melt inclusions in olivines, in primitive magmas derived from small monogenetic cones (MEC) whereas the lowest S contents generally occur in the volcanoes thought to be derived from higher degrees of mantle melting and in the more evolved and larger stratovolcanoes. This disparity in the S content was thought to reflect either the fractionation of S-bearing phases, or to be related to the possibility that the larger stratovolcanoes are likely to experience stronger degassing during ascent though more complex sub-arc plumbing systems compared to the small MEC centers. The  $S_{(90)}$  content for the primitive melts from Melimoyu and Hudson are typical for other larger centers ( $\geq 100\text{ km}^3$ ; Völker et al., 2011) in the SVZ. Mentolat, which is the smallest center in the SSVZ with an edifice volume of  $\sim 36\text{ km}^3$  (Völker et al., 2011), has the highest S contents observed

(Fig. 8B), but this volcano is still much larger ( $\sim 15\text{--}30\times$ ) than any of the MEC, and has erupted more evolved lavas and tephra reflecting a complex subvolcanic plumbing system. Furthermore, based on our melting models, Mentolat is generated by higher degrees of partial melting than the other centers of the SSVZ and thus the  $S_{(90)}$  contents should be diluted similar to the behavior of other incompatible elements, unless it was enriched in the source. Therefore, features such as volcanic size, extent of differentiation and degree of mantle melting are unable alone to explain the elevated  $S_{(90)}$  content of the primitive magmas at Mentolat, and source composition may be an important factor.

### 6.2.2. Chlorine

Wehrmann et al. (2014) observed, a negative correlation between the  $Cl_{(90)}$  content and incompatible trace element ratios that indicate degree of mantle melting and/or source region enrichment (La/Sm; Wehrmann et al., 2014). The lowest  $Cl_{(90)}$  abundances are observed in the volcanoes interpreted to have formed from relatively high-degrees of partial melting (low La/Sm) such that the large stratovolcanoes in the SVZ have lower Cl contents than the smaller MEC which are interpreted to have formed from lower degrees of partial melting. Higher degrees of partial melting act to dilute the concentration of incompatible elements such as Cl. In the SSVZ, the lowest parental  $Cl_{(90)}$  concentrations are found at Melimoyu, Macá and Hudson (Fig. 8B), which erupt magmas that are generated by relatively low degree of partial melting. In contrast, Mentolat which has a higher average  $F_m$  than the other SSVZ centers, has the highest  $Cl_{(90)}$  abundances.

Additionally, Wehrmann et al. (2014) suggest, that there exists an inverse relationship between the size of the volcanic edifice and the Cl abundances (Fig. 8A). Volcanoes with the largest edifice have the lowest  $Cl_{(90)}$  abundances while the smaller centers generally have the highest  $Cl_{(90)}$  contents. The low  $Cl_{(90)}$  contents at Hudson and Melimoyu, which are the largest centers in the southernmost SSVZ, are similar to volcanoes of a comparable size further north in SVZ, while Mentolat, a relatively small center, has  $Cl_{(90)}$  contents similar to the primitive melts from the small mafic cinder cones (MEC) of Apagado, Cabeza de Vaca, and Los Hornitos in the Andean CSVZ (Wehrmann et al., 2014). Thus, the Cl contents of the primitive magmas of the volcanoes of the SSVZ fit the edifice volume model proposed by Wehrmann et al. (2014).

### 6.2.3. Summary

In summary, the melt inclusion S contents may be influenced by two processes: 1) the removal from fractionating S-bearing phases such as apatite or sulfides or, 2) the loss of S through degassing during magmatic differentiation. Thus, the highest S contents are observed in the most primitive magmas which occur at the small volume MEC while the larger stratovolcanoes which have more complex plumbing systems are more likely to experience some degree of degassing or to be impacted by fractionating S-bearing phases. The primitive magma Cl contents were found to correlate negatively with volcanic edifice size, and positively with trace-element proxies for the degree of melting and source composition. Thus, higher degrees of mantle melting

produce a larger volcanic edifice and dilute the concentration of Cl in the primitive melts.

### 6.3. Tectonic factors

One possible explanation for the higher  $F_m$  below Mentolat is a heightened flux of slab derived fluids caused by dehydration of altered oceanic crust within the Guamblyn Fraction Zone which, when projected onto land, traces below Mentolat (Fig. 2). Fracture zones potentially host serpentinite bodies in the altered oceanic crust (Contreras-Reyes et al., 2007, 2008; Manea et al., 2014) and could also provide an efficient means to transport an abundance of hydrous minerals, seawater, and

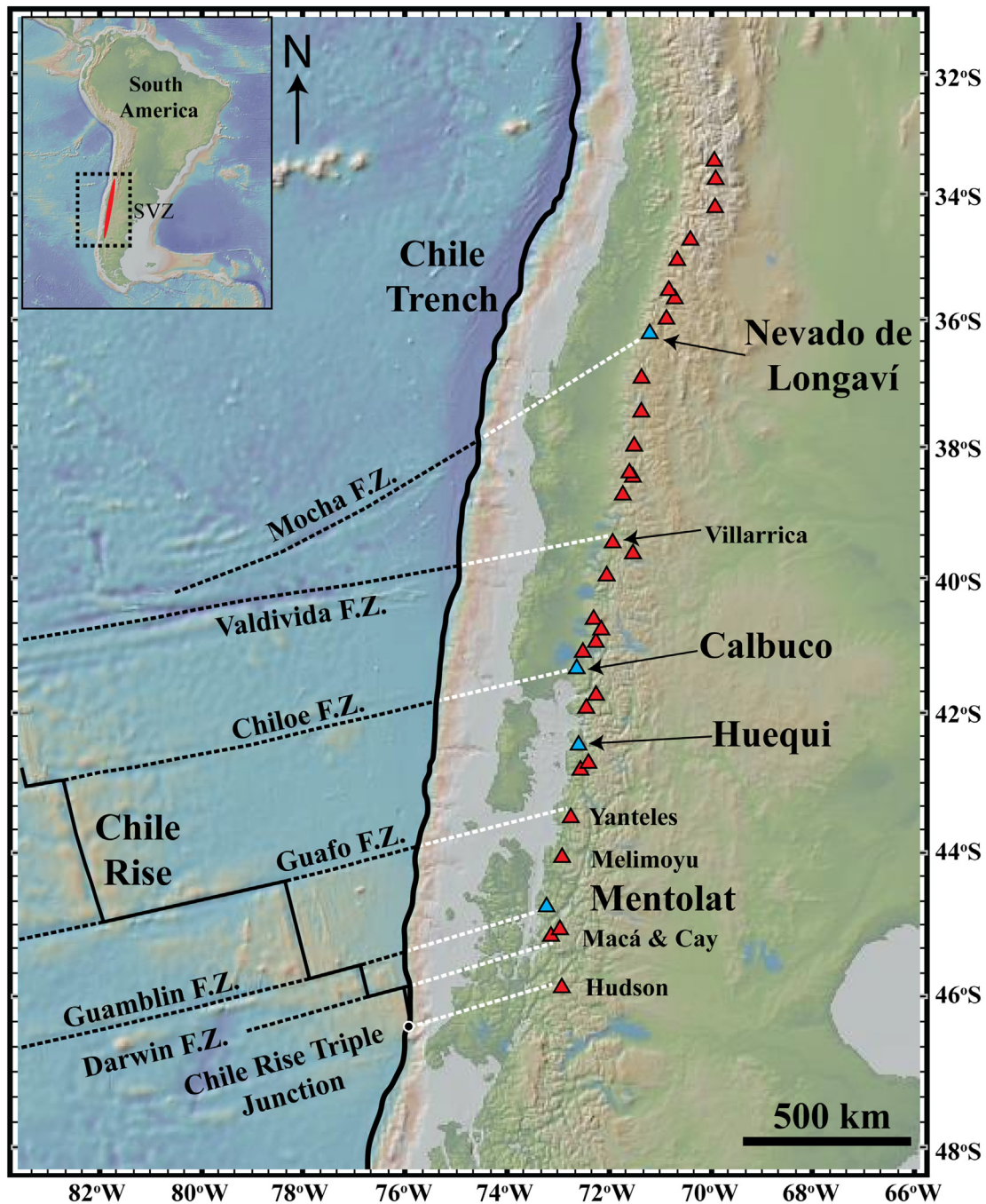


**Fig. 9.** Map showing the location of some of the major Nazca plate fracture zones being subducted below the Andean SVZ and their projected location under the South American continent. Also shown are the volcanoes in the SVZ that have magmas with Very Low Abundance (VLA) characteristics (blue triangles), and with the exception of Huequi, where fracture zone subduction is proposed to impact the chemical characteristics of the eruptive products from these centers. This map was constructed using GeoMapApp (<http://www.geomapp.org>). (For interpretation of the references to color in this figure legend, the reader is referred to the web version of this article.)

sediments into the mantle. An enhanced water flux into the mantle source is also consistent with the presence of amphibole in the eruptive products of Mentolat, while amphibole is rare or absent in lavas or tephros derived from the other centers in the SSVZ (López-Escobar et al., 1993, 1995; Stern et al., 2015, 2016; Weller et al., 2015). Furthermore, Alt et al. (2013) demonstrated that dehydration of serpentinites in subduction zone setting release elevated S contents into the mantle wedge, which could explain the high S content at Mentolat. The elevated  $Cl_{(90)}$  at Mentolat could be the result of enhanced seawater transport into the sub-arc mantle from the highly altered oceanic crust beneath Mentolat. Unfortunately, S or Cl has never been measured in melt inclusion from Nevado de Longaví, Huequi, or Calbuco, those volcanoes in the SVZ that also have unusual VLA magma chemistry similar to Mentolat and also have amphibole as a stable phase (Hickey-Vargas et al., 1995; Rodríguez et al., 2007; Sellés et al., 2004; Watt et al., 2011; Weller et al., 2015).

The influence of fracture zone subduction has been invoked at Nevado de Longaví (Rodríguez et al., 2007; Sellés et al., 2004) further north in the Andean SVZ (Fig. 9). Additionally, Calbuco which is located above the extension of the Chiloe Fracture Zone may also be under the influence of fracture zone subduction (Hickey-Vargas et al., 2016). Both Nevado de Longaví and Calbuco are amphibole-bearing centers that possess the distinctive VLA-type geochemistry of Mentolat (Hickey-Vargas et al., 1995; López-Escobar et al., 1995; Rodríguez et al., 2007; Sellés et al., 2004). However, there is no clear indication of a fracture zone being subducted below Huequi. Furthermore, other prominent Nazca Plate fractures zones such as the Valdivia and Guafu Fracture Zones that occur below areas of the Andean arc near, but not directly below, Villarrica and Yanteles, respectively, without generating amphibole-bearing VLA volcanic centers (Fig. 9).

A special impact for fracture zone subduction has also been suggested for volcanoes in other volcanic arcs world-wide such as Seguam that is situated near the subducting Amlia Fracture Zone in the Aleutian volcanic arc (Singer et al., 2007), Mt. Shasta above the Blanco Fracture Zone in the Cascade arc, and El Chichón and Colima in the Trans-Mexican Volcanic Belt that occur above the Tehuantepec and Rivera Fracture Zones respectively (Manea et al., 2014). Seguam, Mt. Shasta, and Colima are of significance because these centers produce lavas and tephros with relatively low  $K_2O$ ,  $TiO_2$ , and other incompatible trace elements (Grove et al., 2005; Luhr and Carmichael, 1980, 1990; Singer et al., 1996, 2007) similar to the chemical characteristics of Mentolat, Nevado de Longaví, and Calbuco in the Andean SVZ. Also, similar to the other VLA-type centers of the Andean SVZ, Colima (Luhr, 1992) and Mt. Shasta (Grove et al., 2002, 2005) produces amphibole-bearing lavas. To explain the unusual chemistry of the eruptive products at Seguam, Singer et al. (1992) suggest that the Amlia fracture zone transports a larger quantity of slab-derived components such as sediments and hydrous phases beneath the source region. In addition to terrigenous and pelagic sediments, fluids released into the mantle wedge from dehydration of the altered ocean crust within this fracture zone is thought to locally increase the degree of partial melting beneath Seguam, thus generating the VLA-type geochemistry at this center (Singer et al., 1996, 2007). Similarly, higher degrees of partial melting as a result of enhanced fluid input from the subducting slab has also been proposed to explain the magma chemistry at Colima (Luhr, 1992).

An interesting finding from this study is the similarity in the estimated primitive magma compositions for Melimoyu, Macá, and Hudson. Because of its location at the landward projection of the Chile Rise Triple Junction (Fig. 2), previous researches have suggested that the magma chemistry (D'Orazio et al., 2003; Gutiérrez et al., 2005) and heightened eruptive activity (Weller et al., 2014) is related to its unusual tectonic position. Indeed, Hudson is the most active volcanoes in the Andean SSVZ in terms of the frequency and volume of explosive eruptions (Weller et al., 2014, 2015). However, the similarity in the primitive magmas compositions estimated from this study, indicate that magma

genesis at Hudson is more similar to processes occurring at Macá and Melimoyu.

## 7. Conclusions

Olivine-hosted melt inclusions taken from tephros derived from explosive eruptions sampled from lacustrine sediment records downwind of the volcanic front of the southernmost portion of the SSVZ were investigated for pre-eruptive major element and volatile (S and Cl) geochemistry. The melt inclusion compositions were back calculated to primitive magma compositions to assess for the influence of Nazca Plate features such as fracture zones on the generation of magmas in the southernmost SSVZ and to investigate processes generating the geochemical diversity of the eruptive products observed at the surface. Some of the along-strike chemical diversity is also observed in the primitive magmas from these centers, with Mentolat having MgO-poor primitive melts with lower incompatible elements such as  $K_2O$ ,  $TiO_2$ , and higher  $Al_2O_3$ . These features may result from higher degrees of mantle melting, which in turn may be due to an enhanced water transport into the mantle above the subducted Guamblin Fracture Zone causing greater hydrous flux melting in the sub arc mantle beneath Mentolat. The presence of amphibole in the eruptive products indicates relatively high water contents at Mentolat. In contrast, Hudson, Macá, and Melimoyu all have relatively similar parental magma compositions that are MgO-rich, have higher  $K_2O$ ,  $TiO_2$ , and lower  $Al_2O_3$  and are generated by lower degrees of partial melting. The relatively high concentration of  $S_{(90)}$  and  $Cl_{(90)}$  at Mentolat may also be the result of the close proximity beneath Mentolat of the Guamblin Fracture Zone which could efficiently transport hydrous mineral assemblages and potentially sediments and seawater into the subduction zone.

Supplementary data to this article can be found online at <https://doi.org/10.1016/j.lithos.2017.11.009>.

## Acknowledgements

We thank Patricio Moreno, Rodrigo Villa-Martínez, Antonio Maldonado, Eugenia de Porras, Carmen Miranda and Cesar Méndez for access to and information about the lake sediment cores containing the tephra from which the olivines were selected. We would also like to thank two unidentified reviewers for providing many constructive comments that greatly improved the quality of this manuscript.

## References

- Alt, J.C., Schwarzenbach, E.M., Früh-Green, G.L., Shanks III, W.C., Bernasconi, S.M., Garrido, C.J., Crispini, L., Gaggero, L., Padrón-Navarta, J.A., Marchesi, C., 2013. The role of serpentinites in cycling of carbon and sulfur: seafloor serpentinization and subduction metamorphism. *Lithos* 178:40–54. <https://doi.org/10.1016/j.lithos.2012.12.006>.
- Ariskin, A.A., Frenkel, M.Y., Barmina, G.S., Nielsen, R., 1993. COMAGMAT: a FORTRAN program to model magma differentiation processes. *Comput. Geosci.* 19:1155–1170. [https://doi.org/10.1016/0098-3004\(93\)90020-6](https://doi.org/10.1016/0098-3004(93)90020-6).
- Cande, S.C., Leslie, R.B., 1986. Late Cenozoic tectonics of the southern Chile trench. *J. Geophys. Res.* 91 (B1), 471–496.
- Carel, M., Siani, G., Delpéch, G., 2011. Tephrostratigraphy of a deep-sea sediment sequence off the south Chilean margin: new insight into the Hudson volcanic activity since the last glacial period. *J. Volcanol. Geotherm. Res.* 208, 99–111.
- Cembrano, J., Hervé, F., Lavenu, A., 1996. The Liquiñe-Ofqui fault zone: long-lived intra-arc fault system in southern Chile. *Tectonophysics* 259, 55–66.
- Contreras-Reyes, E., Grevemeyer, I., Flueh, E.R., Scherwath, M., Heesemann, M., 2007. Alteration of the subducting oceanic lithosphere at the southern central Chile trench outer rise. *Geochem. Geophys. Geosyst.* 8, 1–19.
- Contreras-Reyes, E., Grevemeyer, I., Flueh, E.R., Reichert, C., 2008. Upper lithospheric structure of the subduction zone offshore of southern Arauco peninsula, Chile, at 38°S. *J. Geophys. Res.* 113.
- Danyushevsky, L.V., Plechov, P., 2011. Petrolog3: integrated software for modeling crystallization processes. *Geochem. Geophys. Geosyst.* 12, Q07021. <https://doi.org/10.1029/2011GC003516>.
- Danyushevsky, L.V., Della-Pasqua, F.N., Sokolov, S., 2000. Re-equilibration of melt inclusions trapped by magnesian olivine phenocrysts from subduction-related magmas: petrological implications. *Contrib. Mineral. Petrol.* 138, 68–83.
- Danyushevsky, L.V., McNeill, A.W., Sobolev, A.V., 2002. Experimental and petrological studies of melt inclusions in phenocrysts from mantle-derived magmas: an overview of techniques, advantages and complications. *Chem. Geol.* 183, 5–24.

- Davidson, J., Turner, S., Handley, H., Macpherson, C., Dosseto, A., 2007. Amphibole "sponge" in the arc crust? *Geology* 35 (9):787–790. <https://doi.org/10.1130/G23637A.1>.
- DeMets, C., Gordon, R.G., Argus, D.F., 2010. Geologically current plate motions. *Geophys. J. Int.* 181, 1–80.
- Devine, J.D., Gardner, J.E., Brack, H.P., Layne, G.D., Rutherford, M.J., 1995. Comparison of microanalytical methods for estimating H<sub>2</sub>O contents of silicic volcanic glasses. *Am. Mineral.* 80, 319–328.
- D'Orazio, M., Innocenti, F., Manetti, P., Tamponi, M., Tonarini, S., González-Ferrán, O., Lahsen, A., 2003. The Quaternary calc-alkaline volcanism of the Patagonian Andes close to the Chile triple junction: geochemistry and petrogenesis of volcanic rocks from the Cay and Maca volcanoes (~45°S, Chile). *J. S. Am. Earth Sci.* 16 (4), 219–242.
- Elbert, J., Wartenburg, R., von Gunten, L., Urrutia, R., Fisher, D., Fújak, M., Hamann, Y., Greber, N.D., Grosjean, M., 2013. Late Holocene air temperature variability reconstructed from the sediments of Laguna Escondida, Patagonia Chile. *Palaeogeogr. Palaeoclimatol. Palaeoecol.* 396, 482–492.
- Ewart, A., 1982. The mineralogy and petrology of Tertiary-Recent orogenic volcanic rocks: with special reference to the andesitic-basaltic compositional range. In: Thorpe, R.S. (Ed.), *Andesites; Orogenic Andesites and Related Rocks*. John Wiley & Sons, Chichester, pp. 25–95.
- Ford, C.E., Russell, D.G., Groven, J.A., Fisk, M.R., 1983. Distribution coefficients of Mg<sub>2</sub> +, Fe<sub>2</sub> +, Ca<sub>2</sub> + and Mn<sub>2</sub> + between olivine and melt. *J. Petrol.* 24, 256–265.
- Futa, K., Stern, C.R., 1988. Sr and Nd isotopic and trace element compositions of Quaternary volcanic centers of the southern Andes. *Earth Planet. Sci. Lett.* 88, 253–262.
- Grove, T.L., Parman, S.W., Bowring, S.A., Price, R.C., Baker, M.B., 2002. The role of an H<sub>2</sub>O-rich fluid component in the generation of primitive basaltic andesites and andesites from the Mt. Shasta region, Northern California. *Contrib. Mineral. Petrol.* 142, 375–379.
- Grove, T.L., Baker, M.B., Price, R.C., Parman, S.W., Elkins-Tanton, L.T., Chatterjee, N., Müntener, O., 2005. Magnesian andesite and dacite lavas from Mt. Shasta, Northern California: products of fractional crystallization of H<sub>2</sub>O-rich mantle melts. *Contrib. Mineral. Petrol.* 148, 542–565.
- Gutiérrez, F., Gioncada, A., González-Ferrán, O., Lahsen, A., Mazzuoli, R., 2005. The Hudson volcano and surrounding monogenetic centres (Chilean Patagonia): an example of volcanism associated with ridge-trench collision environment. *J. Volcanol. Geotherm. Res.* 145, 207–233.
- Hickey-Vargas, R., Mohammad, J.A., Parada, M.A., López-Escobar, L., Frey, F.A., 1995. Crustal xenoliths from Calbuco Volcano, Andean Southern Volcanic Zone: implications for crustal composition and magma-crust interaction. *Contrib. Mineral. Petrol.* 119, 331–344.
- Hickey-Vargas, R., Holbik, S., Tormey, D., Frey, F.A., Moreno Roa, H., 2016. Basaltic rocks from the Andean Southern Volcanic Zone: insight from the comparison of along-strike and small-scale geochemical variations and their sources. *Lithos* 258–259, 115–132.
- Kelley, K.A., Plank, T., Grove, T.L., Stolper, E.M., Newman, S., Hauri, E., 2006. Mantle melting as a function of water content beneath back-arc basins. *J. Geophys. Res.* 111, B09208. <https://doi.org/10.1029/2005JB003732>.
- Kelley, K.A., Plank, T., Newman, S., Stolper, E.M., Grove, T.L., Parman, S., Hauri, E., 2010. Mantle melting as a function of water content beneath the Mariana arc. *J. Petrol.* 51:1711–1738. <https://doi.org/10.1093/petrology/egq036>.
- King, P.L., Vennemann, T.W., Holloway, J.R., Hervig, R.L., Lowenstern, J.B., Forneris, J.F., 2002. Analytical techniques for volatiles: a case study using intermediate (andesitic) glasses. *Am. Mineral.* 87, 1077–1089.
- Kratzmann, D.J., Carey, S., Scasso, R.A., Naranjo, J.A., 2009. Compositional variations and magma mixing in the 1991 eruptions of Hudson volcano, Chile. *Bull. Volcanol.* 71 (4), 419–439.
- Kratzmann, D.J., Carey, S., Scasso, R.A., Naranjo, J.A., 2010. Role of cryptic amphibole crystallization in magma differentiation at Hudson volcano, Southern Volcanic Zone, Chile. *Contrib. Mineral. Petrol.* 159, 237–264.
- Leake, B., Woolley, A., Arps, C., Birch, W., Gilbert, M., Grice, J., Hawthorne, F., Kato, A., Kisch, H., Krivovichev, V., Linthout, K., Laird, J., Mandarino, J., Maresch, W., Nickel, E., Rock, N., Schumacher, J., Smith, D., Stephenson, N., Ungaretti, L., Whittaker, E., Youzhi, G., 1997. Nomenclature of amphiboles: report of the subcommittee on amphiboles of the International Mineralogical Association, Commission on New Minerals and Mineral Names. *Am. Mineral.* 82, 1019–1037.
- López-Escobar, L., Kilian, R., Kempton, P., Tagiri, M., 1993. Petrology and geochemistry of Quaternary rocks from the southern volcanic zone of the Andes between 41°30' and 46°00'S, Chile. *Rev. Geol. Chile* 20, 33–55.
- López-Escobar, L., Parada, M.A., Hickey-Vargas, R., Frey, F.A., Kempton, P., Moreno, H., 1995. Calbuco Volcano and minor eruptive centers distributed along the Liquiñe-Ofqui Fault Zone, Chile (41°S) contrasting origin of andesitic and basaltic magmain the Southern Volcanic Zone of the Andes. *Contrib. Mineral. Petrol.* 119, 345–361.
- Lowenstern, J.B., 1995. Application of silicate melt inclusions to the study of magmatic volatiles. In: Thompson, J.F.H. (Ed.), *Magmas, Fluids and Ore Deposits*. Mineralogical Association of Canada Short Course vol. 23, pp. 71–99.
- Luhr, J.F., 1992. Slab-derived fluids and partial melting in subduction zones: insights from two contrasting Mexican volcanoes (Colima and Ceboruco). *J. Volcanol. Geotherm. Res.* 54, 1–18.
- Luhr, J.F., Carmichael, I.S.E., 1980. The Colima volcanic complex, Mexico. *Contrib. Mineral. Petrol.* 71, 343–372.
- Luhr, J.F., Carmichael, I.S.E., 1990. Petrological monitoring of cyclical eruptive activity at Volcán Colima, Mexico. *J. Volcanol. Geotherm. Res.* 42, 235–260.
- Manea, V.C., Leeman, W.P., Gerya, T., Manea, M., Zhu, G., 2014. Subduction of fracture zones controls mantle melting and geochemical signature above slabs. *Nat. Commun.* 5:5095. <https://doi.org/10.1038/ncomms6095>.
- Morgan, G.B., London, D., 1996. Optimizing the electron microprobe analysis of hydrous alkali aluminosilicate glasses. *Am. Mineral.* 81, 1176–1185.
- Naranjo, J.A., Stern, C.R., 1998. Holocene explosive activity of Hudson Volcano, southern Andes. *Bull. Volcanol.* 59 (4), 291–306.
- Naranjo, J.A., Stern, C.R., 2004. Holocene tephrochronology of the southernmost part (42°30'–45°S) of the Andean Southern Volcanic Zone. *Rev. Geol. Chile* 31 (2), 225–240.
- Naranjo, J.A., Moreno, H.R., Banks, N.G., 1993. La Erupción del Volcán Hudson en 1991 (46°S), Región XI, Aisén, Chile. Servicio Nacional de Geología y Minería. 44 pp. 1–50.
- Notsu, K., López-Escobar, L., Onuma, N., 1987. Along-arc variation of Sr-isotope composition in volcanic rocks from the Southern Andes (33°S–55°S). *Geochem. J.* 21, 307–313.
- Portnyagin, M., Hoernle, K., Plechov, P., Mironov, N., Khubunaya, S., 2007. Constraints on mantle melting and composition and nature of slab components in volcanic arcs from volatiles (H<sub>2</sub>O, S, Cl, F) and trace elements in melt inclusions from the Kamchatka Arc. *Earth Planet. Sci. Lett.* 255:53–69. <https://doi.org/10.1016/j.epsl.2006.12.005>.
- Rodríguez, C., Sellés, D., Dungan, M., Langmuir, C., Leeman, W., 2007. Adakitic dacites formed by intracrustal crystal fractionation of water-rich parent magmas at Nevado de Longavi (36.2°S; Andean Southern Volcanic Zone, Central Chile). *J. Petrol.* 48 (11), 2033–2061.
- Salteras, V.J.M., Stracke, A., 2004. Composition of the depleted mantle. *Geochem. Geophys. Geosyst.* 5, Q05B07. <https://doi.org/10.1029/2003GC000597>.
- Sellés, D., Rodríguez, C.A., Dungan, M.A., Naranjo, J.A., Gardeweg, M., 2004. Geochemistry of Nevado de Longavi (36.2°S): a compositionally atypical volcano in the Southern Volcanic Zone of the Andes. *Rev. Geol. Chile* 31 (2), 293–315.
- Singer, B.S., Myers, J.D., Frost, C.D., 1992. Mid-Pleistocene lava from the Segum volcanic center, central Aleutian arc: closed-system fractional crystallization of a basalt to rhyodacite eruptive suite. *Contrib. Mineral. Petrol.* 110, 87–112.
- Singer, B.S., Leeman, W.P., Thirlwall, M.F., Rogers, N.W., 1996. Does fracture zone subduction increase sediment flux and mantle melting in subduction zones? Trace element evidence from Aleutian arc basalt. In subduction top to bottom. *Geophys. Monogr.* 96.
- Singer, B.S., Jicha, B.R., Leeman, W.P., Rogers, N.W., Thirlwall, M.F., Ryan, J., Nicolaysen, K.E., 2007. Along-strike trace element and isotopic variation in Aleutian Island arc basalt: subduction melts sediments and dehydrates serpentine. *J. Geophys. Res.* 112. <https://doi.org/10.1029/2006JB004897>.
- Stern, C.R., 2004. Active Andean volcanism: its geologic and tectonic setting. *Rev. Geol. Chile* 31 (2), 161–206.
- Stern, C.R., 2008. Holocene tephrochronology record of large explosive eruptions in the southernmost Patagonian Andes. *Bull. Volcanol.* 70 (4), 435–454.
- Stern, C.R., de Porras, M.E., Maldonado, A., 2015. Tephrochronology of the upper Río Cisnes valley (44°S), southern Chile. *Andean Geol.* 42 (2), 173–192.
- Stern, C.R., Moreno, P.I., Henrique, W.I., Villa-Martínez, R.P., Sagredo, E., Aravena, J.C., De Pol-Holz, R., 2016. Holocene tephrochronology in the area around Cochane, southern Chile. *Andean Geol.* 43 (1), 1–19.
- Stolper, E., Newman, S., 1994. The role of water in the petrogenesis of Mariana trough magmas. *Earth Planet. Sci. Lett.* 121, 293–325.
- Vargas, G., Rebollo, S., Sepúlveda, S.A., Lahsen, A., Thiele, R., Townley, B., Padilla, C., Rauld, R., Herrera, M.J., Lara, M., 2013. Submarine earthquake rupture, active faulting and volcanism along the major Liquiñe-Ofque Fault Zone and implications for seismic hazard assessment in the Patagonian Andes. *Andean Geol.* 40, 141–171.
- Völker, D., Kutterolf, S., Wehrmann, H., 2011. Comparative mass balance of volcanic edifices at the southern volcanic zone of the Andes between 33°S and 46°S. *J. Volcanol. Geotherm. Res.* 205, 114–129.
- Wallace, P.J., 2005. Volatiles in subduction zone magmas: concentrations and fluxes based on melt inclusions and volcanic gas data. *J. Volcanol. Geotherm. Res.* 140:217–240. <https://doi.org/10.1016/j.volgeores.2004.07.23>.
- Wallace, P.J., Edmonds, M., 2011. The sulfur budget in magmas: evidence from melt inclusions, submarine glasses, and volcanic gas emissions. *Rev. Mineral. Geochem.* 73, 215–246.
- Watt, S.F.L., Pyle, D.M., Mather, T.A., 2011. Geology, petrology and geochemistry of the dome complex of Huequi volcano, southern Chile. *Andean Geol.* 38 (2), 335–348.
- Watt, S.F.L., Pyle, D.M., Mather, T.A., Naranjo, J.A., 2013. Arc magma compositions controlled by linked thermal and chemical gradients above the subducting slab. *Geophys. Res. Lett.* 40 (11), 2550–2556.
- Wehrmann, H., Hoernle, K., Jacques, G., Garbe-Schönberg, D., Schumann, K., Mahlke, J., Lara, L., 2014. Sulphur and chlorine geochemistry of mafic to intermediate tephros from the Chilean Southern Volcanic Zone (33–43°S) compared with those from the Central American Volcanic Arc. *Int. J. Earth Sci.* 103, 1945–1962.
- Weller, D.J., Miranda, C.G., Moreno, P.I., Villa-Martínez, R.P., Stern, C.R., 2014. A large late-glacial Ho eruption for the Hudson volcano, southern Chile. *Bull. Volcanol.* 76, 831–849.
- Weller, D.J., Miranda, C.G., Moreno, P.I., Villa-Martínez, R.P., Stern, C.R., 2015. Tephrochronology of the Andean Southern Volcanic Zone. *Chile. Bull. Volcanol.* 76, 831–849.
- Weller, D.J., de Porras, E., Maldonado, A., Stern, C.R., 2017a. Holocene tephrochronology of the lower Río Cisnes Valley, southern Chile. *Andean Geol.* 44 (3), 229–248.
- Weller, D.J., de Porras, E., Maldonado, A., Stern, C.R., 2017b. New age controls on the tephrochronology of the southernmost Andean Southern Volcanic Zone, Chile. *Bull. Volcanol.* (under review).